Mechanism for Catechol Ring Cleavage by Non-Heme Iron Intradiol Dioxygenases: A Hybrid DFT Study

2 AUTHORS, INCLUDING:

Tomasz Borowski

Instytut Katalizy i Fizykochemii Powierzchni i…

45 PUBLICATIONS   **1,215** CITATIONS

Mechanism for Catechol Ring Cleavage by Non-Heme Iron Intradiol Dioxygenases: A Hybrid DFT Study

Tomasz Borowski*,† and Per E. M. Siegbahn*,‡

Contribution from the Institute of Catalysis and Surface Chemistry, Polish Academy of Sciences, ul. Niezapominajek 8, 30-239 Cracow, Poland, and Department of Physics, Stockholm Center for Physics, Astronomy and Biotechnology, Stockholm University, S-106 91 Stockholm, Sweden.

Received June 12, 2006; E-mail: ncborows@cyf-kr.edu.pl; ps@physto.se

Abstract: The mechanism of the catalytic reaction of protocatechuate 3,4-dioxygenase (3,4-PCD), a representative intradiol dioxygenase, was studied with the hybrid density functional method B3LYP. First, a smaller model involving only the iron first-shell ligands (His460, His462, and Tyr408) and the substrates (catechol and dioxygen) was used to probe various a priori plausible reaction mechanisms. Then, an extended model involving also the most important second-shell groups (Arg457, Gln477, and Tyr479) was used for the refinement of the preselected mechanisms. The computational results suggest that the chemical reactions constituting the catalytic cycle of intradiol dioxygenases involve: (1) binding of the substrate as a dianion, in agreement with experimental suggestions, (2) binding of dioxygen to the metal aided by an electron transfer from the substrate to O_2, (3) formation of a bridging peroxo intermediate and its conformational change, which opens the coordination site trans to His462, (4) binding of a neutral XOH ligand (H_2O or Tyr447) at the open site, (5) proton transfer from XOH to the neighboring peroxo ligand yielding the hydroperoxo intermediate, (6) a Criegee rearrangement leading to the anhydride intermediate, and (7) hydrolysis of the anhydride to the final acyclic product. One of the most important results obtained is that the Criegee mechanism requires an in-plane orientation of the four atoms (two oxygen and two carbon atoms) mainly involved in the reaction. This orientation yields a good overlap between the two σ orbitals involved, C–C σ and O–O σ^*, allowing an efficient electron flow between them. Another interesting result is that under some conditions, a homolytic O–O bond cleavage might compete with the Criegee rearrangement. The role of the second-shell residues and the substituent effects are also discussed.

1. Introduction

Protocatechuate 3,4-dioxygenase (3,4-PCD) is an Fe^{III}-dependent enzyme involved in biodegradation of aromatic compounds.[1] It catalyzes the oxidative ring scission of protocatechuate (PCA; 3,4-dihydroxybenzoate) to β-carboxy-*cis,cis*-muconic acid, which means that the ring is specifically cleaved at the C–C bond between the two carbon atoms binding the hydroxyl groups (C3 and C4, see Scheme 1). This type of ring scission is known as intradiol cleavage, as opposed to the *extradiol* type effected by Fe^{II}-dependent dioxygenases cleaving the ring at the C–C bond adjacent to the enediol functionality, i.e., the C2–C3 or C4–C5. The literature on both types of diol dioxygenases is very rich, and we refer interested readers to excellent reviews on the subject.[2−9] From a broader perspective, the chemistry of intradiol dioxygenases is interesting for several

Scheme 1. Reaction Catalyzed by Protocatechuate 3,4-Dioxygenase

PCA : protocatechuate : 3,4-dihydroxybenzoate

β-carboxy-cis,cis-muconic acid
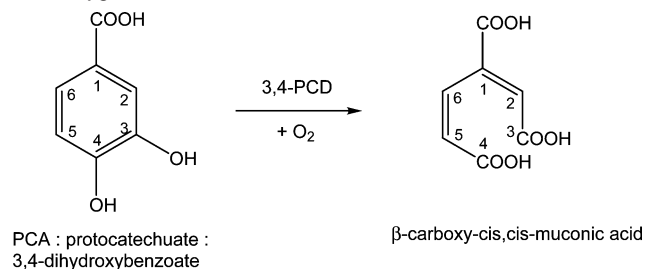
reasons. First, a unique mechanism of catechol ring activation through coordination to ferric ion has been proposed for this class of enzymes. Second, the mechanism of the Criegee rearrangement, which is a key step of the catalytic cycle, is still elusive. Among others, these two aspects are discussed in this paper from the theoretical perspective, and it is believed that new valuable insights have been provided by the DFT study reported here.

Intradiol dioxygenases form a relatively small but well-studied group of enzymes. The wealth of structural and spectroscopic

† Polish Academy of Sciences.
‡ Stockholm Center for Physics.
(1) Fujisawa, H.; Hayaishi, O. *J. Biol. Chem.* **1968**, *243*, 2673−2681.
(2) Brown, C. K.; Vetting, M. W.; Earhart, C. A.; Ohlendorf, D. H. *Annu. Rev. Microbiol.* **2004**, *58*, 555−585.
(3) Costas, M.; Mehn, M. P.; Jensen, M. P.; Que, L. *Chem. Rev.* **2004**, *104*, 939−986.
(4) Que, L., Jr.; Ho, R. Y. N. *Chem. Rev.* **1996**, *96*, 2607−2624.
(5) Ryle, M. J.; Hausinger, R. P. *Curr. Opin. Chem. Biol.* **2002**, *6*, 193−201.
(6) Bugg, T. D. H. *Tetrahedron* **2003**, *59*, 7075−7101.
(7) Bugg, T. D. H. *Curr. Opin. Chem. Biol.* **2001**, *5*, 550−555.
(8) Bugg, T. D. H.; Winfield, C. J. *Nat. Prod. Rep.* **1998**, 513−530.

(9) Solomon, E. S.; Brunold, T. C.; Davis, M. I.; Kemsley, J. N.; Lee, S. K.; Lehnert, N.; Neese, F.; Skulan, A. J.; Yang, Y. S.; Zhou, J. *Chem. Rev.* **2000**, *100*, 235−349.

Scheme 2. Reaction Mechanism Proposed by Ohlendorf et al.[2] for 3,4-PCD
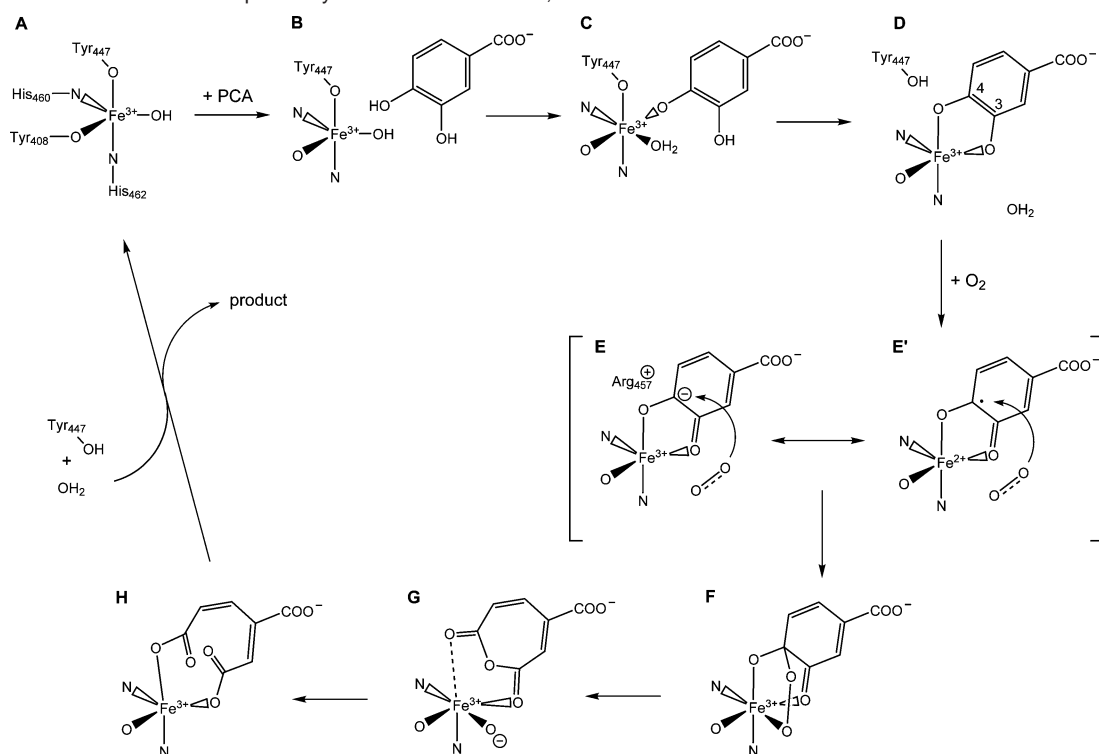
data available for 3,4-PCD favors this particular enzyme to be considered as a representative for this group. The crystal structure of the native form of 3,4-PCD reveals that the ferric ion at the active site is coordinated by four endogenous and one solvent ligand that adopt a trigonal bipyramidal arrangement around the metal.[10] Accordingly, in the equatorial plane, there are tyrosinate (Tyr408), histidine (His460), and the solvent-derived OH group, and the two axial ligands are tyrosinate (Tyr447) and another histidine (His462). The two tyrosinates form distinct Fe−O bonds, as demonstrated in the spectroscopic studies.[11,12] The mode of substrate binding was probed in the EPR investigations, showing that the substrate chelates the high-spin ferric ion[13] and that the water-derived ligand is absent in the iron coordination sphere in the 3,4-PCD−PCA (enzyme−substrate) complex.[14] The resonance Raman studies on anaerobic enzyme−substrate complex of catechol 1,2-dioxygenase, i.e., an intradiol dioxygenase with an active site very similar to 3,4-PCD, showed that the substrate binds to Fe(III) as a dianion.[15] Similarly, the visible spectrum of the enzyme−inhibitor complex is consistent with the dianionic form of 4-nitrocatechol (4-NC), a potent competitive inhibitor of 3,4-PCD.[16]

Structural data obtained for complexes of 3,4-PCD with various ligands has provided insight into a plausible mechanism of the early stages of the catalytic reaction (from **A** to **D** in

Scheme 2).[2,17] The initial steps involve: binding of the substrate within the active site (**A** → **B**), deprotonation of the C4-bound hydroxyl group by the Fe-bound hydroxide (**B** → **C**),[17] and deprotonation of the C3-bound hydroxyl by the tyrosinate Tyr447. Both water and Tyr447 dissociate from the ferric ion upon the substrate chelation to the metal (**C** → **D**).[18] Interestingly, three structures with an axial tyrosinate (Tyr447) bound to iron and the substrate coordinating the metal only with the C4-bound oxygen were recently reported for 3,4-PCD mutants obtained by the replacement of the equatorial tyrosine (Tyr408) with other amino acids.[19] Thus, these new structures resemble intermediate **C**, but in the coordination sphere of iron there is no water ligand and the arrangement around the metal is trigonal bipyramidal instead of octahedral.

The mechanism of chemical transformations following the substrate binding (**D** → **H**) is still not fully understood. It was proposed that chelation of the substrate to Fe^III activates it for an electrophilic attack by dioxygen, which leads to the formation of a peroxo bridge between iron and C4 (**F**). The equatorial tyrosinate (Tyr408) is proposed to facilitate the ketonization of the C3−O bond, through a trans effect, and does in this way direct the attack of dioxygen at C4. The second-shell arginine (Arg457) is supposed to stabilize the carbanion produced by the C3−O bond ketonization, and thus act together with Tyr408 in directing the electrophilic attack of O_2. As an alternative for the direct attack of dioxygen on the bound substrate, some authors propose that the catechol dianion is one-electron oxidized by Fe^III, which leads to an Fe^II-semiquinone species **E′**, somewhat less stable than **E** because the spectroscopic results

(10) Ohlendorf, D.; Orville, A.; Lipscomb, J. *J. Mol. Biol.* **1994**, *244*, 586−608.
(11) Davis, M. I.; Orville, A. M.; Neese, F.; Zaleski, J. M.; Lipscomb, J. D.; Solomon, E. I. *J. Am. Chem. Soc.* **2002**, *124*, 602−614.
(12) Siu, D.; Orville, A.; Lipscomb, J.; Ohlendorf, D.; Que, L. *Biochemistry* **1992**, *31*, 10443−10448.
(13) Orville, A.; Lipscomb, J. *J. Biol. Chem.* **1989**, *264*, 8791−8801.
(14) Whittaker, J.; Lipscomb, J. *J. Biol. Chem.* **1984**, *259*, 4487−4495.
(15) Horsman, G. P.; Jirasek, A.; Vaillancourt, F. H.; Barbosa, C. J.; Jarzecki, A. A.; Xu, C.; Mekmouche, Y.; Spiro, T. G.; Lipscomb, J. D.; Blades, M. W.; Turner, R. F. B.; Eltis, L. D. *J. Am. Chem. Soc.* **2005**, *127*, 16882−16891.
(16) Tyson, C. A. *J. Biol. Chem.* **1975**, *250*, 1765−1770.

(17) Orville, A.; Elango, N.; Lipscomb, J.; Ohlendorf, D. *Biochemistry* **1997**, *36*, 10039−10051.
(18) Orville, A.; Lipscomb, J.; Ohlendorf, D. *Biochemistry* **1997**, *36*, 10052−10066.
(19) Valley, M. P.; Brown, C. K.; Burk, D. L.; Vetting, M. W.; Ohlendorf, D. H.; Lipscomb, J. D. *Biochemistry* **2005**, *44*, 11024−11039.

A

B
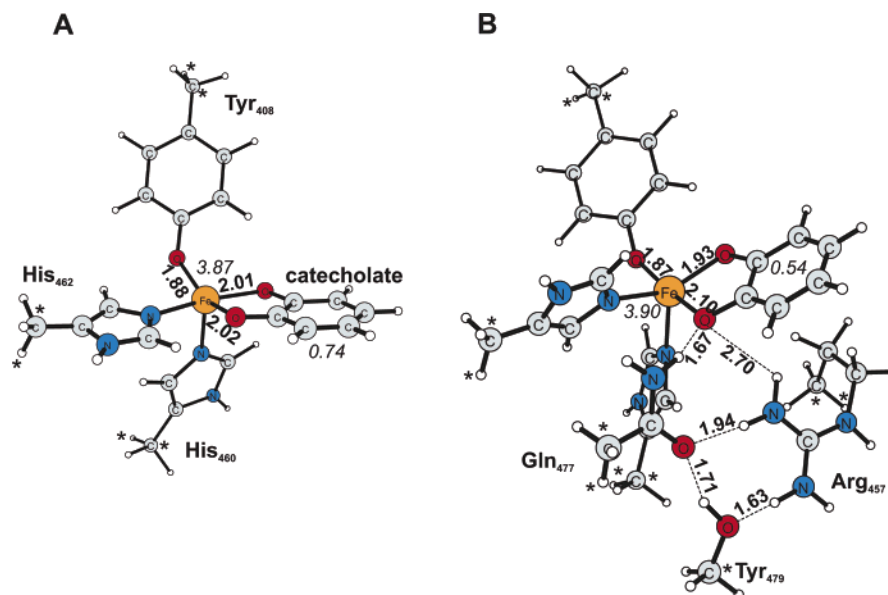
Figure 1. The optimized structures for (A) the smaller model of the enzyme−substrate complex and (B) the bigger model for this species (**1**). Distances in Å in bold, spin populations in italics, atoms marked with asterisks were constrained to their positions in the crystal structure.

suggest that iron remains in the ferric state throughout the catalytic cycle.[3,15,20] Due to the ferrous oxidation state, this intermediate might bind dioxygen to the metal and then the attack on the ring would lead to intermediate **F**. **F** would undergo a Criegee rearrangement (acyl migration to the peroxo oxygen) leading to the anhydride/$Fe^{III}-O^-$ intermediate **G**, which decays to the final product complex **H** through a nucleophilic attack of the O-anion at the anhydride.

Kinetic studies for the native 3,4-PCD have provided rate constants for the four resolved steps in the catalytic cycle: substrate binding (2×10^6 M^{-1} s^{-1}), dioxygen binding to the enzyme−substrate (E−S) complex (5×10^5 M^{-1} s^{-1}), transformation of the ternary E−S−O_2 complex into the oxygenated intermediate E−S−O_2^* (450 s^{-1}), and the final step(s) including product release (36 s^{-1}).[21] Kinetic studies for a Y447H mutant of 3,4-PCD indicated that the absence of the axial tyrosine does not affect the rate of the chemical steps of the catalytic cycle but significantly slows down the substrate binding, which supports the proposal that Tyr447 is involved only in the substrate binding and product release steps.[22] Interesting data pertinent to the mechanism of the chemical steps were provided by the kinetic studies employing substituted catechols.[23,24] These investigations showed that electron-donating substituents accelerate the reaction, whereas electron-withdrawing groups slow it down. Similarly, 6-chlorination of PCA was shown to decrease the rate of dioxygen binding, whereas the next step was hardly affected.[25]

Concerning the product specificity, catechol 1,2-dioxygenase was reported to oxidize 3-substituted catechols into a mixture of products, where the dominating one originates from the usual *intra* cleavage, and the chemical structure of the minority species indicated *extra* scission.[26]

(20) Funabiki, T.; Yamazaki, T. *J. Mol. Cat. A* **1999**, *150*, 37−47.
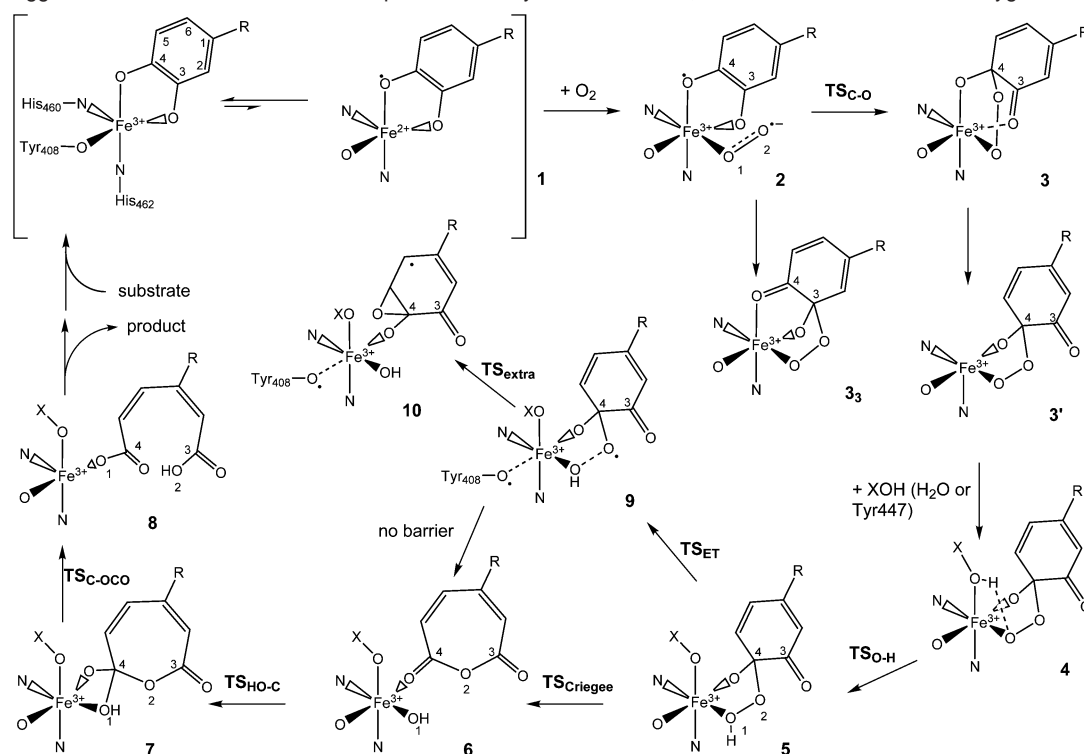(21) Bull, C.; Ballou, D.; Otsuka, S. *J. Biol. Chem.* **1981**, *256*, 12681−12686.
(22) Frazee, R.; Orville, A.; Dolbeare, K.; Yu, H.; Ohlendorf, D.; Lipscomb, J. *Biochemistry* **1998**, *37*, 2131−2144.
(23) Dorn, E.; Knackmuss, H.-J. *Biochem. J.* **1978**, *174*, 85−94.
(24) Walsh, T. A.; Ballou, D. P.; Mayer, R.; Que, L., Jr. *J. Biol. Chem.* **1983**, *258*, 14422−14427.
(25) Walsh, T. A.; Ballou, D. *J. Biol. Chem.* **1983**, *258*, 14413−14421.

In the present paper, the results of hybrid DFT calculations for the mechanism of the catalytic reaction of 3,4-PCD are reported. The computational results indicate that the enzyme−substrate complex has a substantial amount of Fe^{II}-semiquinonate character (**E′** in Scheme 2), which aids dioxygen binding to the metal. Once the E−S−O_2 complex is formed, an easy attack of the O_2 ligand on C4 leads to the peroxo-bridged intermediate (**F**). The calculated energetics for various plausible reactions of species **F** suggest that the productive decay of this intermediate requires protonation of the peroxo group. It is proposed that the source of the proton is a neutral ligand (water or Tyr447) that binds to the iron and dissociates to an Fe^{III}-bound anion and a proton delivered to the peroxo bridge. Two mechanisms of O−O bond cleavage were found to involve similar barriers: a Criegee rearrangement with a synchronous C−C and O−O bond cleavage directly yielding the anhydride intermediate, and a homolytic pathway that involves a metastable radical species. The substituent effects and a plausible role of Arg457 are also discussed.

2. Computational Details

The models of the 3,4-PCD active site are based on the crystal structure solved for the enzyme complexed with 2-hydroxyisonicotinic acid *N*-oxide and cyanide (PDB code: 3PCL).[18] The inhibitor molecule was replaced with an unsubstituted catechol, whereas cyanide was either omitted or replaced with dioxygen. Two models differing in size were employed in the calculations. First, a smaller system (ca. 55 atoms, see Figure 1A) comprising the iron first-shell ligands (His460, His462, Tyr408, and catechol) was used. Histidines are modeled with methylimidazoles, Tyr408 with a 4-methylphenol anion; the bonds cut were saturated with hydrogens. Restrained optimizations were performed with the atoms corresponding to Cα and Cβ in the His and Tyr408 residues constrained to their positions in the crystal structure. In this way, the rigidity of the protein backbone was taken into account in the model. With this model, various mechanism were tested. The second bigger model (ca. 90 atoms, see Figure 1B) is an extension of the smaller one in which the possibly important second-shell residues (Arg457, Gln477)

(26) Fujiwara, M.; Golovleva, L.; Saeki, Y.; Nozaki, M.; Hayaishi, O. *J. Biol. Chem.* **1975**, *250*, 4848−4855.

Scheme 3. Suggested Mechanism for Chemical Steps in the Catalytic Reaction of 3,4-PCD and Other Intradiol Dioxygenases

and their H-bonding partner (Tyr479) are also included. The model of Arg457 includes the entire side chain, for Gln477 the Cβ is replaced with a hydrogen, whereas Tyr479 is modeled with a methanol molecule. With this model, only selected mechanisms, found with the smaller model to involve the lowest barriers, were reinvestigated. The total charge of the smaller model is zero, whereas the bigger model has a +1 charge.

All calculations were performed employing hybrid DFT with the B3LYP exchange-correlation functional.[27,28] Two programs, Gaussian03[29] and Jaguar,[30] were used. Geometry optimizations were done with a valence double-ζ basis set coupled with an effective core potential describing the innermost electrons on iron. This particular basis set is labeled lacvp in Jaguar. For the optimized structures, the electronic energy was computed with a bigger basis set of triple-ζ quality with polarization functions on all atoms (labeled lacv3p** in Jaguar). The solvent corrections were calculated with the self-consistent reaction field method implemented in Jaguar.[31,32] A dielectric constant of 4 and a probe radius of 1.4 Å were used to model the protein surrounding of the active site. Zero energy corresponds to the isolated reactants in their ground states, i.e., the model of the 3,4-PCD-catechol complex in the sextet spin state and the triplet molecular dioxygen.

3. Results and Discussion

The computational results suggest that the catalytic cycle of 3,4-PCD involves the following major steps (Scheme 3): dioxygen binding yielding the peroxo-bridged intermediate (**1,2** and **3**); a conformational change creating a vacant site at the axial position (**3** and **3'**); binding and a subsequent splitting of

(27) Becke, A. D. J. *Chem. Phys.* **1993**, *98*, 5648−5652.
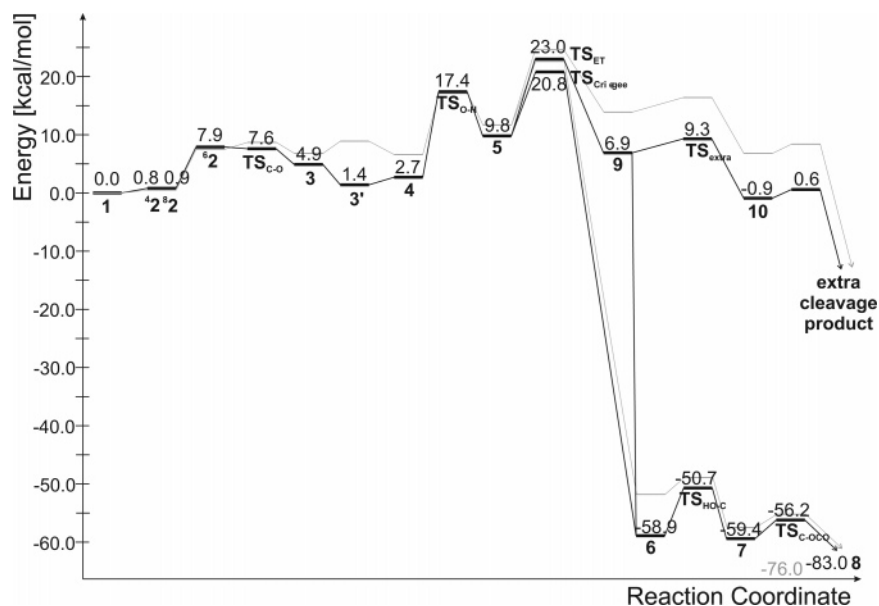(28) Lee, C.; Yang, W.; Parr, R. G. *Phys. Rev.* **1988**, B37, 785−789.
(29) Frisch, M. J. et al. *Gaussian 03*, revision B. 03; Gaussian Inc.: Pittsburgh, PA, 2003.
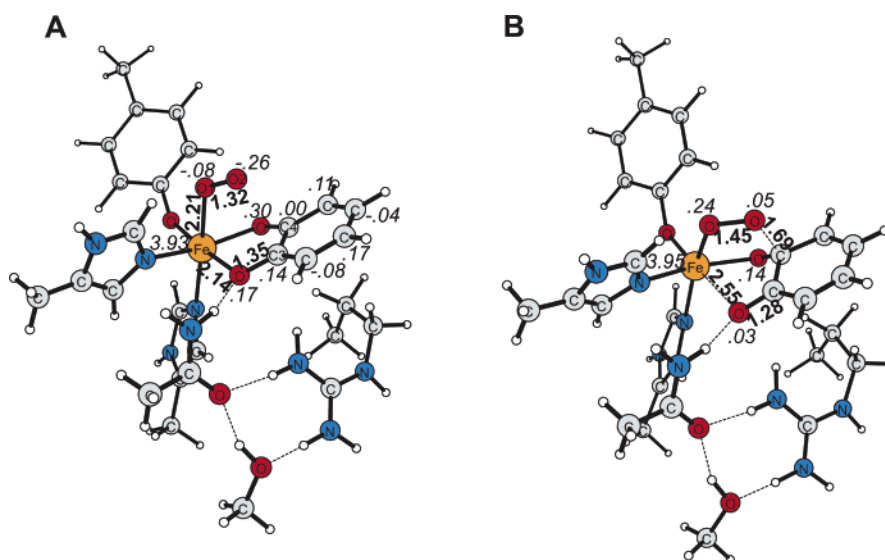(30) *JAGUAR 5.5*; Schrödinger, Inc.: Portland, OR, 2005.
(31) Tannor, D. J.; Marten, B.; Murphy, R.; Friesner, R. A.; Sitkoff, D.; Nicholls, A.; Ringnalda, M.; Goddard, W. A., III; Honig, B. *J. Am. Chem. Soc.* **1994**, *116*, 11875−11882.
(32) Marten, B.; Kim, K.; Cortis, C.; Friesner, R. A.; Murphy, R.; Ringnalda, M.; Sitkoff, D.; Honig, B. *J. Phys. Chem.* **1996**, *100*, 11775−11788.

a neutral ligand (water or Tyr447), which produces a hydroperoxo intermediate (**4** and **5**); heterolytic (**TS**$_{Criegee}$) or homolytic (**TS**$_{ET}$) cleavage of the O−O bond leading to an anhydride intermediate **6**; and the final hydrolysis of **6** to the product complex **8**. Except for the initial dioxygen binding, the rest of the catalytic cycle takes place on the sextet potential energy surface (PES). It is proposed that the catalytic role of the second-shell Arg457 is to promote the conformational change (**3** → **3'**), which is critical for the mechanism. The detailed discussion of the mechanism and the calculated energetics (Figure 2) is presented in the following subsections.

3.1. Substrate and Dioxygen Activation. Once the substrate is bound and chelates iron as a dianion (**1** in Scheme 3), it gains substantial radical (semiquinonate) character. This partial one-electron oxidation of the substrate by the ferric ion is manifested in the spin populations reported for the E−S complexes in Figure 1. The total spin population on the substrate is 0.74 and 0.54 for the smaller and bigger model, respectively, whereas the spin population on iron has values intermediate between those typical for high-spin ferrous and ferric non-heme complexes. Thus, the presence of the second-shell residues in the bigger model stabilizes the ferric/dianion resonance structure. From the bond lengths reported, one can notice that the asymmetry in substrate binding observed in the crystal structure[18] is reproduced with the bigger model: the Fe−O bond trans to Tyr408 is 0.17 Å longer than the other one.

The presence of the ferrous/semiquinonate resonance in the electronic structure of the E−S complex is critical for the next catalytic step, i.e., dioxygen binding; a proposal already present in the literature.[3,15,20] The computational results described at the end of this manuscript and previous theoretical studies[20] indicate that the direct attack of triplet dioxygen at the substrate is unlikely. On the other hand, the partial ferrous character of the iron enables a direct binding of dioxygen to the metal. On

Figure 2. Calculated energy profile along the suggested reaction path for 3,4-PCD. Black: bigger model, gray: smaller model.
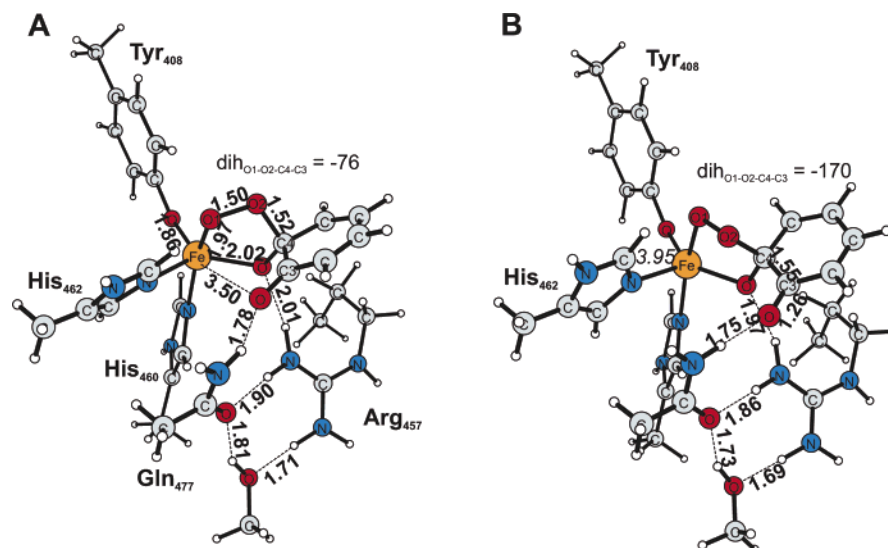

Figure 3. The optimized structures for (A) the ternary enzyme—substrate-O_2 complex in the sextet spin state (^{6}**2**) and (B) the transition state for the attack of the O_2 ligand on the ring (C4 carbon atom) (**TS**$_{C-O}$). Distances in Å in bold, spin populations in italics.

the quartet and octet PES:s, which are directly accessible for the reactants (the sextet E—S complex and triplet dioxygen), dioxygen is weakly (0.8 and 0.9 kcal/mol) unbound in the E—S—O_2 complexes (^{4}**2**, ^{8}**2** Figure 2, and Supporting Information). Once these end-on complexes are formed, an intersystem crossing to the sextet spin state (^{6}**2**) is possible, because this process is endothermic by only 7 kcal/mol (for a comparison, the sextet → quartet intersystem crossing in the E—S complex was computed to be endothermic by 15.6 kcal/mol). Starting from ^{6}**2** the rest of the catalytic cycle takes place on the sextet PES. From the spin populations calculated for this ternary complex (Figure 3A) one can notice that its electronic structure corresponds to a semiquinonate ligand and the Fe^{II}—O_2/Fe^{III}—O_2^- moiety. Importantly, the unpaired electrons on semiquinonate and superoxide have opposite spins, a feature facilitating the C—O bond formation discussed below.

3.2. Formation of the Peroxo Intermediate and Opening of the Axial Coordination Site. Opposite spins on superoxide

and semiquinonate help substantially in the development of a chemical bond between the two fragments of ^{6}**2**. Indeed, the transition state for this process, i.e., attack of the distal oxygen (O2) on carbon C4 of the substrate, was optimized (**TS**$_{C-O}$, Figure 3B) and the activation energy calculated with the bigger basis set is only 2.6 kcal/mol (small basis: 2.7 kcal/mol). However, the solvent effects stabilize this TS with respect to ^{6}**2** by 2.9 kcal/mol, which renders the C-O bond formation to be a spontaneous process once the sextet spin state is reached by the ternary E—S—O_2 complex. Similarly, the activation barrier calculated with the smaller model is also close to zero (1.2 kcal/mol, Figure 2). From the structure and spin populations calculated for **TS**$_{C-O}$ it can be recognized that already at the TS geometry the electron is transferred from the semiquinonate to the superoxide, which becomes a peroxo group. At the same time, the C3—O bond is ketonized (shortened from 1.35 to 1.28 Å) and the Fe—O bond engaging this group is substantially elongated (from 2.14 to 2.55 Å). These features are fully

Figure 4. The optimized structures for two conformations of the peroxo-bridged intermediate: (A) species **3** obtained directly in the attack of O2 at C4 and (B) species **3′** with the accessible coordination site trans to His462. Distances in Å in bold, spin populations in italics.

expressed in the product of this step, i.e., the peroxo-bridged intermediate **3** shown in Figure 4A. Notably, the C3-bound ketone oxygen is very far (3.5 Å) from iron and the arrangement of the ligands around the metal is approximately trigonal bipyramidal with the peroxo group and His460 being the axial ligands. The equatorial Tyr408−Fe−O(−C4) angle is 121 degrees. Quite interestingly, for the smaller model, which lacks the second-shell ligands, the geometry of this intermediate is much closer to distorted octahedral: the keto group is markedly closer to the metal (2.51 Å), and the equatorial Tyr408−Fe−O(−C4) angle is 110 degrees. Thus, from the comparison of these two structures, one might speculate that Arg457 and Gln477 pull the C4-bound oxygen toward Gln477 and in this way open the coordination site trans to His462, i.e., the original axial site where Tyr447 binds to Fe^{III} before substrate binding. Indeed, this structural observation is further supported by the calculated energetics for the conformational change that opens this site completely (**3** → **3′**, see Figure 4). This process involves opening of the Tyr408−Fe−O(−C4) angle to 135 degrees and the change of the O1−O2−C4−C3 dihedral angle from −76 to −170 degrees (values for the bigger model). This transformation is exothermic by 3.5 kcal/mol for the bigger model, whereas it is endothermic by 2.1 kcal/mol for the smaller model, which means that the second-shell residues provide 5.6 kcal/mol stabilization energy for the open structure **3′**. This is an important effect because, as discussed below, the open site trans to His462 is the place where the neutral ligand (water or Tyr447) binds to the metal; a process critical for the progress of the catalytic reaction. The stabilization effect of the second shell residues most likely comes from enhanced hydrogen bonding in species **3′**. Indeed, it can be noticed in Figure 4 that all hydrogen bonds present in the complex are strengthened when going from 3 (Figure 4A) to **3′** (Figure 4B), and thus, strengthening of these five hydrogen bonds is proposed to contribute the 5.6 kcal/mol stabilization energy. Because Arg457 is a charged residue and it takes a central place in the H-bond network, i.e., it mediates the interaction between the negatively charged oxygen atom of the substrate and Gln477 and Tyr479, it is suggested that this residue plays a pivotal role in the conformational change leading from **3** to **3′**.

Scheme 4. Test System for the Energetics of Dioxygen Binding
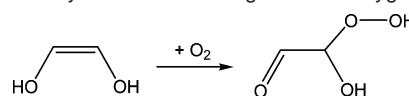
Finally, a few comments should be given about the calculated energetics of dioxygen binding. First, the energy profile presented in Figure 2 does not include entropy effects. Entropy effects are expected to be very similar for all points except the starting point with a free dioxygen. The additional entropy of this point should be around 10 kcal/mol. When dioxygen becomes bound there is a compensating effect which should be added to the energy curve. In comparison to accurate calculations and experiments, it is the experience that the electronic structure method employed in this study (B3LYP/lacv3p**// B3LYP/lacvp) has a tendency to underestimate the enthalpy of binding of dioxygen and other small molecules, partly because of missing van der Waals effects in DFT. For example, the calculated energy of dioxygen binding to the enediol molecule (see Scheme 4) is −27.4 kcal/mol for B3LYP, whereas in the more accurate method, CBS-QB3,[33] it is −33.3 kcal/mol. Thus, in this test case, the B3LYP underestimates the energy of O2 binding by 5.9 kcal/mol. An additional effect comes from van der Waals binding of dioxygen to the protein. For simplicity, it has here been assumed that entropy and these other additional effects essentially cancel, which is why entropy has not been included in the figure. Still, it is clear that the curve describing the initial binding of dioxygen is not very accurate. However, from the point where dioxygen has been bound, it is probably a good approximation to assume that entropy effects are constant and that B3LYP has a similar and high accuracy (see the comparison below for O−O bond cleavage of a small model). This means that the main mechanistic conclusions should be valid. An improved description of the energetics of dioxygen binding would still be desirable but would require substantial method developments, including an extension of the functional to include van der Waals effects, and development of gradient methods based on free energies rather than enthalpies.

(33) Montgomery, J., Jr.; Frisch, M.; Ochterski, J.; Petersson, G. *J. Chem. Phys.* **1999**, *110*, 2822−2827.
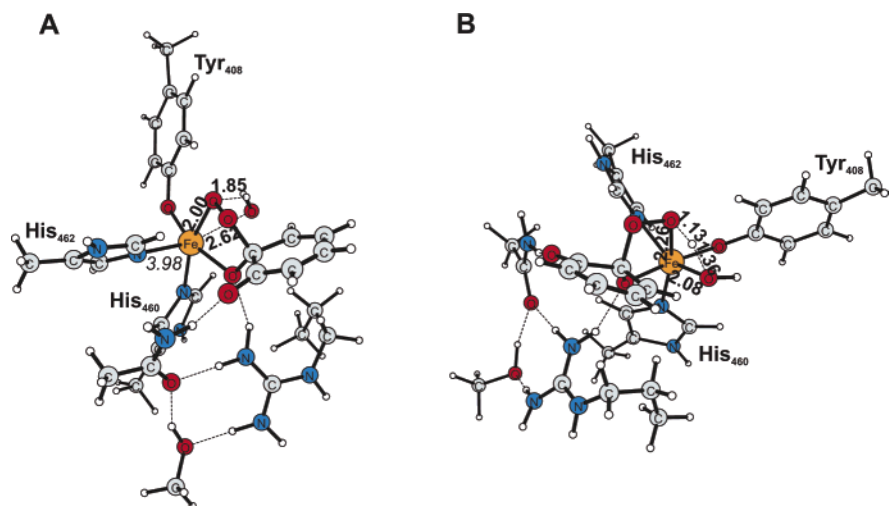
Figure 5. The optimized structures for (A) the peroxo-bridged intermediate with a water molecule bound at the site trans to His462 (**4**) and (B) the transition state for a proton transfer between the water and peroxo ligands (**TS**$_{O-H}$). Distances in Å in bold, spin populations in italics.

3.3. Binding of a Neutral Ligand and Its Dissociation. Structural data available for intradiol dioxygenases indicate that iron with its bound ligands tend to preserve a total neutral charge.[18] In the E−S complex, the formal +3 charge of iron is compensated by the −2 charge of the substrate and −1 from Tyr408. Binding of a charge-neutral dioxygen to the E−S yielding **3′** maintains this charge state. However, the exploration of the PES for the peroxo-bridged intermediate, **3′** and **3** discussed in full length below, indicates that the progress of the catalytic reaction requires that the peroxo oxygen bound to iron is protonated, i.e., without this proton available, reactions involve high barriers and/or are highly endothermic. Because there is no obvious source of this proton in the crystal structures, and taking into account the tendency of the 3,4-PCD active site to preserve the charge, it is proposed that a neutral ligand, such as water or Tyr447, binds to the open coordination site of **3′**, i.e., trans to His462—the original axial site occupied by Tyr447 in the native form of the enzyme. Subsequently, this new XO−H ligand provides a proton to the peroxo group and the XO⁻ anion compensates for the loss of negative charge on the peroxide (**4** → **5** in Scheme 3). The energy of such a proton transfer can be estimated form the known pKa values for H_2O_2 and H_2O (11.62 and 15.7, respectively) if one assumes that the difference in binding energy, between Fe^{III} and RO⁻ and Fe^{III} and ROH, is similar for water and hydroperoxide. This estimate is 5.6 kcal/mol, which is not too far from the calculated value of 7.1 kcal/mol (**4** → **5**, *vide infra*). Because the calculations performed with a smaller model show that binding of a phenol molecule or water leads to very similar results, only the water-bound models are discussed here.

Binding of a water molecule at the open coordination site of **3′** is computed to be slightly endothermic (1.3 kcal/mol), mostly due to the desolvation of water (Figure 2). However, it should be noted that the energy of water binding (**3′** → **4**) might, in reality, be more favorable than the value reported here. The reason is that the axial site, i.e., the place where the water binds, is most solvent exposed among the coordination sites around iron. Thus, it is likely that the water ligand, when bound to iron, is markedly better solvated than the continuum solvent method suggests. A definite confirmation of this suggestion would require a QM/MM study.

In the water-bound intermediate **4**, shown in Figure 5A, the water ligand forms a hydrogen bond with the peroxo oxygen and a long coordination bond with iron. Both of these interactions facilitate the proton transfer to the peroxo ligand, since as can be noticed from Figure 5B, depicting the optimized transition state **TS**$_{O-H}$, this proton shift strengthens the Fe−OX bond. The proton transfer involves a barrier of 16.0 kcal/mol, is endothermic by 8.4 kcal/mol (calculated with respect to **3′**, see Figure 2), and leads to the hydroperoxo intermediate **5** presented in Figure 6A. Interestingly, an indirect evidence supporting the formation of such an intermediate comes from the comparison of its structure with the geometry of the active site region in the recently published mutant complex (Figure 7).[19] In this structure (PDB code: 1YKP), the equatorial Tyr408 is replaced by histidine, which is unable to approach the iron and binds to the metal only indirectly through a water (Wat901) ligand. Importantly, in this mutant, the axial Tyr447 does not dissociate from iron during the substrate binding, which leads to the E−S complex with the occupied axial site and a monodentate binding mode for the substrate. These features make this E−S complex very similar to the hydroperoxo intermediate **5**. Indeed, in Figure 7, one can notice that except for the interchange in the positions of the water-derived and tyrosinate ligands and the obvious lack of the hydroperoxo group in the E−S complex, the two structures are close to each other. Most importantly, the configuration of the substrate groups are almost identical, as are the positions of the second-shell residues: Arg457 and Gln477. Accordingly, taking together the energetics and structural data, it seems that the formation of species **5** is a viable path for the intradiol catalytic reaction. The decay of **5** toward the intradiol cleavage product is discussed in the following subsection.

**3.4. Heterolytic and Homolytic O−O Bond Cleavage.** Aside from providing the place for the X−OH ligand, the opening of the axial coordination site trans to His462 results in a change of the dihedral angle defined by the peroxo oxygens and the C4 and C3 carbons in the substrate ring (O1−O2−

---

(34) Humphrey, W.; Dalke, A.; Schulten, K. *J. Mol. Graph.* **1996**, *14*, 33−38.
(35) *Persistence of Vision Raytracer*, version 3.6; Persistence of Vision Pty. Ltd.: Williamstown, Victoria, Australia, 2004; retrieved from http://www.povray.org/download/.
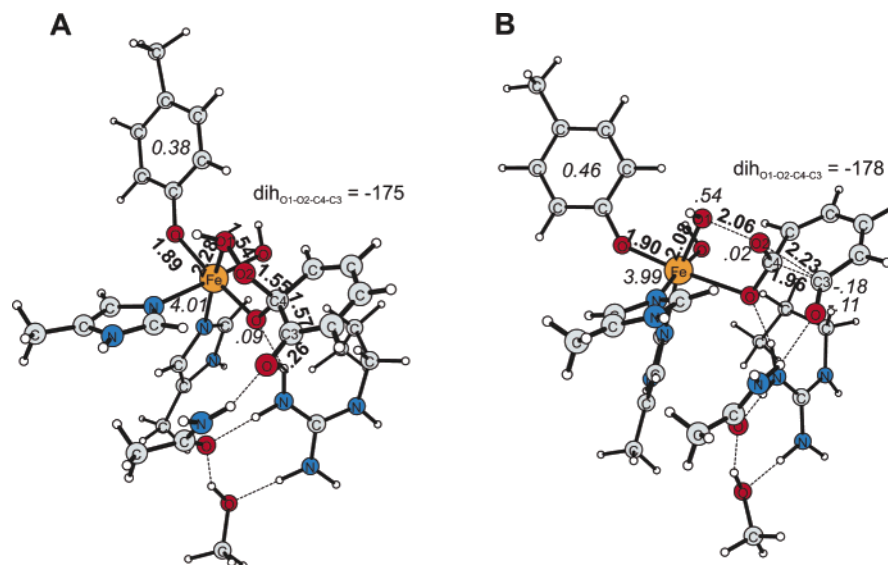
Figure 6. The optimized structures for (A) the hydroperoxo intermediate with a OH$^-$ anion bound at the site trans to His462 (**5**) and (B) the transition state for the Criegee rearrangement (**TS**$_{Criegee}$). Distances in Å in bold, spin populations in italics.
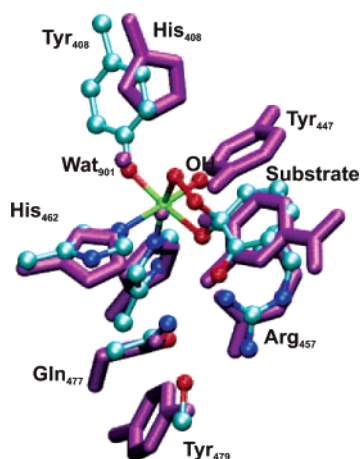
Figure 7. Overlay of the X-ray crystal structure for the active site in the Y408H + PCA complex (PDB code: 1YKP[19]) (magenta) and the optimized structure of **5** (ball-and-stick, hydrogens omitted for clarity). The figure was produced with VMD[34] and PovRay.[35]

C4−C3, Scheme 3). This angle changes from −76 degrees in **3** to −170 in **3′**, and after water binding and dissociation, it has a value of −175 in **5**. This seemingly unimportant geometrical change is pivotal for the progress of the catalytic reaction. Namely, only for such an in-plane arrangement of the four atoms it is possible to optimize a transition state for a Criegee rearrangement: for **TS**$_{Criegee}$ shown in Figure 6B, the dihedral is −178 degrees. Comparing the two structures presented in Figure 6, one can recognize that the Criegee rearrangement involves simultaneous O1−O2 and C3−C4 bond cleavage concerted with formation of a bond between O2 and C3. Moreover, the calculated spin populations indicate that only a small amount of spin builds up on the substrate and the spins on iron and Tyr408 are almost unaffected. This, in turn, indicates that the reaction is a heterolytic process with the HO$^-$ leaving group and the insertion of the formal O$^+$ into the C4−C3 bond. The HO$^-$ group forms a bond with the ferric ion and the insertion of the O2 oxygen atom into the ring leads to an anhydride intermediate **6** presented in Figure 8A. The calculated energy for **TS**$_{Criegee}$ is 20.8 kcal/mol with respect to the reactants,

which means that the activation barrier calculated from **5** is only 11 kcal/mol. Formation of the anhydride intermediate **6** is irreversible, because the calculated energy for this species is −58.9 kcal/mol with respect to the reactants (Figure 2).

The requirement for the in-plane arrangement of the four atoms (O1, O2, C4, and C3) during the Criegee rearrangement stems from the character of the electronic structure changes during this process. More specifically, the heterolytic O−O bond cleavage renders the O2 atom electron deficient; it is formally an O$^+$ ion with an empty valence orbital. This orbital points along the O2−O1 bond vector and originates from the O−O σ^* in **5**. The "O$^+$" ion develops a bond with C3 at the same time as the C3−C4 bond is cleaved, which means that the electrons of the C−C σ bond are shifted and used for establishing the C−O bond. Efficient electron flow requires a good overlap between the two σ orbitals (O−O σ^* and C−C σ), and this is guaranteed by the in-plane arrangement of the four atoms (see Scheme 5).

To visualize these changes in the electronic structure, the TS of the Criegee rearrangement was optimized for a small organic model, which contains only the groups indispensable for the progress of this reaction (Figure 9A). The optimized structure of this TS and its Kohn−Sham HOMO are shown in Figure 9B and C, respectively. The shape of the HOMO clearly indicates a strong mixing between the O−O σ^* and the C−C σ orbitals, which illustrates the flow of the electrons between the two sigma orbitals discussed above. Moreover, for this small system, the activation energy calculated with the B3LYP and CBS-QB3 methods are 23.6 and 24.4 kcal/mol, respectively, which shows that B3LYP provides a quite accurate barrier for the Criegee rearrangement. In this small model system the leaving HO$^-$ group has no partner to bind to, so once the TS is passed, HO$^-$ attacks the anhydride, which leads to its spontaneous hydrolysis to a HCOOH−OOCH complex. The energy of this reaction calculated with B3LYP and CBS-QB3 is −112.9 and −107.8 kcal/mol respectively, which implies a 5.1 kcal/mol difference.

(36) Portmann, S.; Lüthi, H. P. *CHIMIA* **2000**, *54*, 766−770.

A **B**
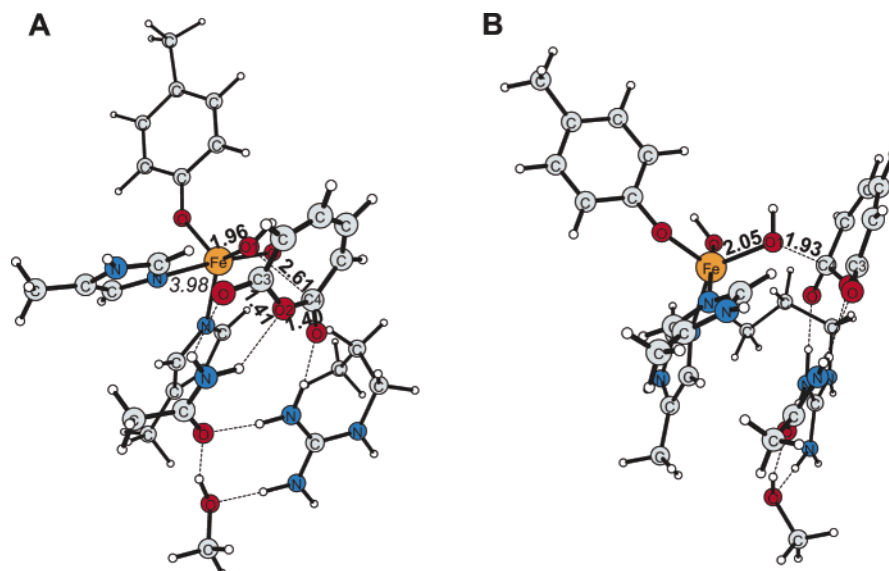
Figure 8. Optimized structures for (A) the anhydride intermediate (**6**), and (B) the transition state for the attack of the Fe-bound OH group on the carbonyl carbon of the anhydride (TS_{HO-C}). Distances in Å in bold, spin populations in italics.

Scheme 5. Schematic Representation of the Orbital Overlap Requirement for Criegee Rearrangement

Previous DFT studies on the reaction mechanisms of extradiol dioxygenases have shown that a homolytic HO−OR bond cleavage is usually coupled with an electron transfer from Fe^{II} or Mn^{II} ions to the hydroperoxo group.[37−39] In this way, the leaving OH radical is reduced to an HO^- anion bound to Fe^{III} or Mn^{III}, whereas the R−O• radical easily forms an epoxide radical intermediate. A similar process can be envisioned for intradiol dioxygenases. However, in the hydroperoxo intermediate **5** iron has a ferric oxidation state, which means it is a much weaker reductant compared to Fe^{II}. On the other hand, tyrosinate Tyr408 seems to be a viable electron donor. Indeed, a TS for O−O bond homolysis coupled to the electron transfer from Tyr408 to the peroxo group was found and its structure is shown in Figure 10A, and the spin density calculated for this TS is presented in Figure 10B. From the spin populations and the spatial spin-density plot, it is evident that an oxygen radical develops on O2, the tyrosinate is oxidized to a tyrosine radical, while the leaving OH radical is reduced to Fe^{III}-bound HO^- anion. This is also clearly manifested in the structure and spin populations obtained for the product of that step, i.e., **9** shown in Figure 10C. The calculated activation energy for the TS_{ET} is only 2.2 kcal/mol higher than that obtained for the Criegee rearrangement, but the reaction energies are dramatically different: the Criegee rearrangement is extremely exothermic, whereas the homolytic O−O cleavage is only 2.9 kcal/mol downhill (Figure 2). Interestingly, from the computational results it follows that the formation of the radical intermediate would not affect the product specificity of 3,4-PCD, because **9** is

unstable with respect to C4−C3 bond cleavage. This bond scission coupled with O2−C3 and Tyr408−Fe bond formation leads to an anhydride intermediate **6**. The reason for this spontaneous intra cleavage is again traced back to the orbital symmetry. Due to the in-plane arrangement of the O1−O2 and C4−C3 bonds, the singly occupied orbital on O2, which lies along the O1−O2 bond vector (see Figure 10B), interacts with the sigma C4−C3 bonding orbital and weakens this carbon−carbon bond; e.g., its length is 1.61 Å already in **9** (Figure 10C). On the other hand, the formation of the extra epoxide radical **10**, which could evolve toward the extradiol cleavage product, involves a barrier of 2.4 kcal/mol (Scheme 3 and Figure 2, for structures see Supporting Information). This relatively small difference between the activation barriers for the intra and extra cleavage of the catechol ring following the homolytic O−O bond cleavage might provide an explanation for the fact that for some catechols a mixture of intra and extra cleavage products were observed.[26]

Taken together, both heterolytic and homolytic paths, involving $TS_{Criegee}$ or TS_{ET}, lead to the formation of the cyclic anhydride intermediate **6**, whose hydrolysis to the final acyclic product is discussed in the next subsection.

3.5. Hydrolysis of the Anhydride Intermediate. Once the anhydride intermediate **6** is formed, the red-ox chemistry of the 3,4-PCD catalytic reaction is completed, and the final stage of the cycle is a hydrolysis of the anhydride by the hydroxide anion formed in the O−O bond cleavage step. In Figure 8A, it can be noticed that the HO^- anion involving the dioxygen-derived atom O1 is in close proximity of the anhydride carbon C4, the distance between the two atoms is only 2.61 Å. This arrangement facilitates an efficient addition of the OH group to the ring and its subsequent cleavage, which guarantees the dioxygenase stoichiometry of the catalytic reaction. In other words, both atoms derived from dioxygen are incorporated into the acyclic product **8** (Scheme 3). The attack of the OH group at C4 leads through TS_{HO-C} shown in Figure 8B and involves an activation barrier of 8.2 kcal/mol (Figure 2). The low activation barrier is associated with an early character of this TS, i.e., the O1−C4 distance is fairly large (1.93 Å). Addition of the

(37) Siegbahn, P. E. M.; Haeffner, F. *J. Am. Chem. Soc.* **2004**, *126*, 8919−8932.
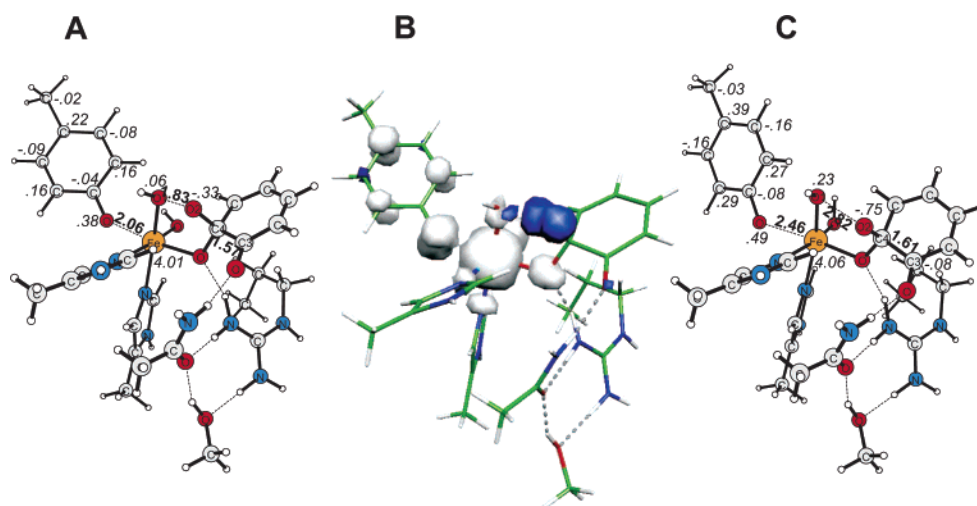(38) Borowski, T.; Georgiev, V.; Siegbahn, P. E. M. *J. Am. Chem. Soc.* **2005**, *127*, 17303−17314.
(39) Georgiev, V.; Borowski, T.; Siegbahn, P. E. M. *J. Biol. Inorg. Chem.* **2006**, *11*, 571−585.
(40) Sawaki, Y.; Ogata, Y. *J. Am. Chem. Soc.* **1975**, *97*, 6983−6989.
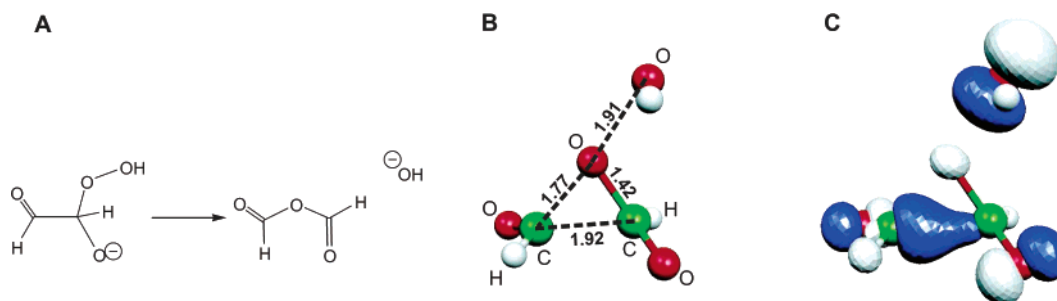
Figure 9. (A) Minimal model for the Criegee rearrangement, (B) optimized TS for this model, and (C) plot of the HOMO KS orbital for the TS. The figure was produced with MOLEKEL.[36]

Figure 10. (A) Transition state for homolytic O−O bond cleavage coupled with an electron transfer from Tyr408 to the O−O bond (TS_{ET}), (B) plot of spin density calculated for the TS_{ET}, and (C) radical metastable intermediate (**9**). Distances in Å in bold, spin populations in italics.
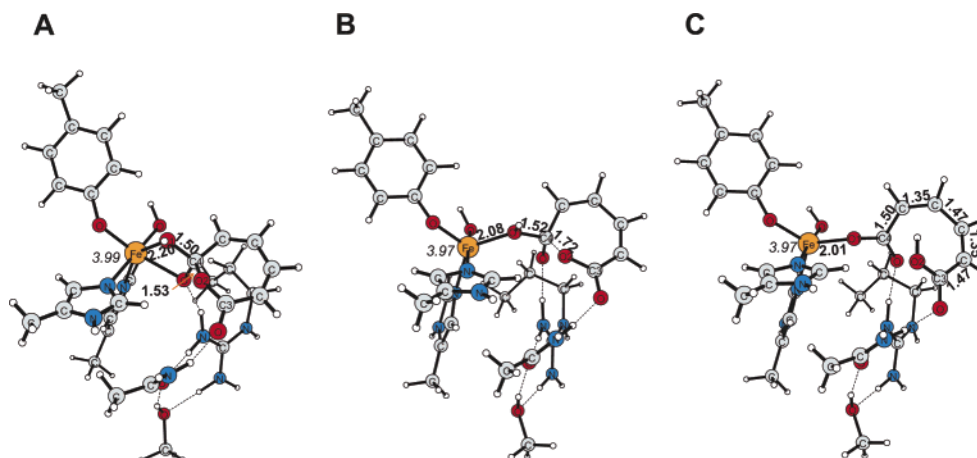
Figure 11. Optimized structures for (A) the tetrahedral intermediate obtained in a nucleophilic attack of the OH group at C4 of the anhydride (**7**), (B) the optimized TS for a cleavage of the tetrahedral intermediate (TS_{C-OCO}), and (C) the final acyclic product complex (**8**). Distances in Å in bold, spin populations in italics.

hydroxide to C4 forms a tetrahedral intermediate **7** (Figure 11A), which is only 0.5 kcal/mol more stable than **6**. The formation of the tetrahedral center at C4 elongates the C4−O2 bond from 1.40 in **6** to 1.53 Å in **7**. Further elongation of this bond to 1.72 Å leads to a transition state for the final ring cleavage (TS_{C-OCO}, Figure 11B) and involves an activation barrier of only 3.2 kcal/mol (Figure 2). In the product of this step (**8** shown in Figure 11C), which is 23.6 kcal/mol more stable than **7**, the carboxylic group involving C4 is deprotonated and forms a coordination bond with Fe^{III} and a hydrogen bond with Arg457, whereas the C3-based carboxylic group is protonated and forms

a hydrogen bond with Gln477. At this stage, the chemical part of the catalytic reaction is completed. The product release, not addressed in this work, finalizes the catalytic cycle.

3.6. Substituent Effects. Catechol and PCA are two natural substrates for intradiol dioxygenases, which differ by the substituent R attached to the C1 carbon in the aromatic ring, i.e., R = H or COO$^-$ for catechol and PCA, respectively (Scheme 3). A potent competitive inhibitor of intradiol dioxygenases is 4-nitrocatechol, R = NO$_2$. Thus, it is interesting to investigate the effect of substitution of hydrogen by either COO$^-$ or NO$_2$ on the calculated energetics of the proposed reaction mechanism.

This was done only for a smaller model (without the second-shell residues) and only for selected structures along the reaction coordinate. Moreover, the substituent effects are discussed based on differences in electronic energies because the relative solvent effects are supposed to be similar upon the change of R.

The changes in the energy of the peroxo-bridged intermediate **3** with respect to the reactants (**1** + O_2) should express the impact of the substitution on the reactivity of **1** toward dioxygen. In agreement with the electro-donating and electro-withdrawing nature of COO^- and NO_2, respectively, the energy of **3** for R = COO^- is 10.1 kcal/mol lower than for the unsubstituted catechol, whereas for R = NO_2, **3** is destabilized by 8.8 kcal/mol. These stabilizing and destabilizing effects with respect to the reactants remain similar for the hydroperoxo intermediate **5**, though the effect of COO^- is markedly reduced (to −5.0 kcal/mol), whereas the effect of NO_2 is almost unchanged (+7.9 kcal/mol). Concerning the effect on the O−O cleavage step, for the substituted compounds, it was possible to optimize only one TS for each substituent. More specifically, for R = COO^-, the Criegee TS ($TS_{Criegee}$) was found, whereas for R = NO_2, only the TS_{ET} was found. The reason for this is most likely a strong impact of the substituents on the energy of the Criegee rearrangement TS. Namely, for R = COO^-, $TS_{Criegee}$ is stabilized by 12.1 kcal/mol, which should be compared with 5 kcal/mol obtained for **5**, and a destabilization similar in magnitude might be expected for R = NO_2. On the other hand, for R=NO_2, TS_{ET} is destabilized with respect to the reactants by 6.2 kcal/mol, which is close to +7.9 kcal/mol obtained for **5**. Thus, whereas the barrier for Criegee rearrangement, calculated with respect to **5**, is sensitive to the substitution in the ring, the homolytic path is largely unaffected. Such a behavior is not surprising if one takes into account the fact that during the Criegee rearrangement, the electrons flow from the ring to the peroxide, whereas during the homolytic O−O cleavage, the electron is provided by tyrosinate Tyr408, and the electrons of the ring are not directly involved. Thus, the heterolytic (Criegee) mechanism is strongly preferred for electron-donating groups like COO^-, whereas the homolytic path will be favored for electron withdrawing groups. However, for NO_2, due to the high energy of the hydroperoxo species **5**, the estimated activation energy for O−O cleavage, leading through TS_{ET}, is 29.2 (23.0 + 6.2), which renders this reaction extremely slow at room temperature. This explains why 4-nitrocatechol is not oxidized by intradiol dioxygenases.

In summary, the substituents affect the steps engaging the electrons of the ring: dioxygen addition leading to the peroxo intermediate and the Criegee rearrangement, whereas the homolytic O−O cleavage is insensitive to the changes of R. The electron-donating groups activate the ring, whereas the electron-withdrawing make the ring less reactive toward O_2 addition and oxygen atom insertion (Criegee rearrangement). These observations are in agreement with available experimental data.[23,24]

3.7. Side Reaction and Alternative Mechanisms. The mechanism presented above involves the attack of the O_2 group at C4 leading to **3**. The alternative attack at C3 was also considered, and the product of this reaction **3$_3$** (Scheme 3) was optimized. Interestingly, the calculated energy for **3$_3$** is 4.4 kcal/mol, which means that this species is slightly more stable than **3**, by 0.5 kcal/mol. The important difference between **3$_3$** and **3**

is that the former has an octahedral geometry around the iron, whereas the latter is closer to trigonal bipyramidal with no bond between the ketonized C−O group and iron and the partially open coordination site trans to His462. Furthermore, in an exothermic process, **3** changes its conformation to **3′**, in which the most solvent accessible site (trans to His462) is empty and the O1−O2−C4−C3 dihedral angle assumes a value close to −180 degrees; both factors, as discussed above, are important for the progress of the catalytic reaction. The driving force for this change is provided by the second-shell residues, which pull the C4-bound negative oxygen to the site trans to Tyr408. In the case of **3$_3$**, the negative oxygen (bound to C3) is already in that position, forming hydrogen bonds with Gln477 and Arg457, and thus, no driving force for opening the site trans to His462 is available. Thus, if **3$_3$** is formed, it is most likely a dead-end product, which has to decay back into **6$_2$** and then evolve toward **3′** (Scheme 3).

Several mechanistic alternatives to the one described above were tested with the smaller model of the active site, but all of them involved markedly higher barriers or reaction energies (Scheme 6). First, the direct attack of dioxygen at the substrate was probed (Scheme 6A). Such a direct attack can take place only on the quartet or octet PES, since these two spin states correspond to antiferromagnetic or ferromagnetic coupling between the unpaired electrons of the ground state reactants: sextet **1** and triplet dioxygen. However, like in a previous computational study,[20] it was found that the PES for such an attack of O_2 at C4 is very repulsive. Optimization with the C4−O2 distance constrained to 1.55 Å gave very high energies: 32.6 and 25.2 kcal/mol for octet and quartet, respectively. Taking into account that the excitation of **1** into the quartet spin state requires 15.6 kcal/mol, it seems that the mechanism suggested above for dioxygen binding is most likely correct.

The second alternative considered was the direct decay of the peroxo intermediate **3** without the protonation of the proximal oxygen atom (Scheme 6B, C). Because no Criegee TS was found for species **3** and **3′**, it was tested if the anhydride formation could be a two-step process. However, the energies calculated for the O1−O2 and C3−C4 cleavage products are very high: 28.5 and 33.6 kcal/mol, respectively (Scheme 6B). The mechanism involving the dioxethane-like TS is also unlikely due to the high activation energy for this process (39.5 kcal/mol, Scheme 6C).

Finally, it was checked if a neutral ligand (H_2O or Tyr447) could add to **3** or **3$_3$** and in this way facilitate a concerted C−C and O−O bond cleavage, a process different from the Criegee rearrangement because it would lead directly to the acyclic product (Scheme 6D, E).[24,40] However, also in this case, the calculated activation barriers are prohibitively high: 31.8 and 36.4 kcal/mol.

4. Conclusions

The presented computational results indicate that the chemical steps in the catalytic cycle of intradiol dioxygenases involve (see Scheme 3): (1) binding of dioxygen to iron, which leads to species **2** with a semiquinonate radical and a superoxide ion coordinated to Fe^{III}, (2) an attack of the superoxide on the C4 carbon in the semiquinonate radical yielding the peroxo-bridged intermediate **3**, (3) a conformational change of **3** to **3′** opening the coordination site trans to His462 and changing the value of

Scheme 6. Alternative Mechanisms for Intradiol Dioxygenases Considered in This Work
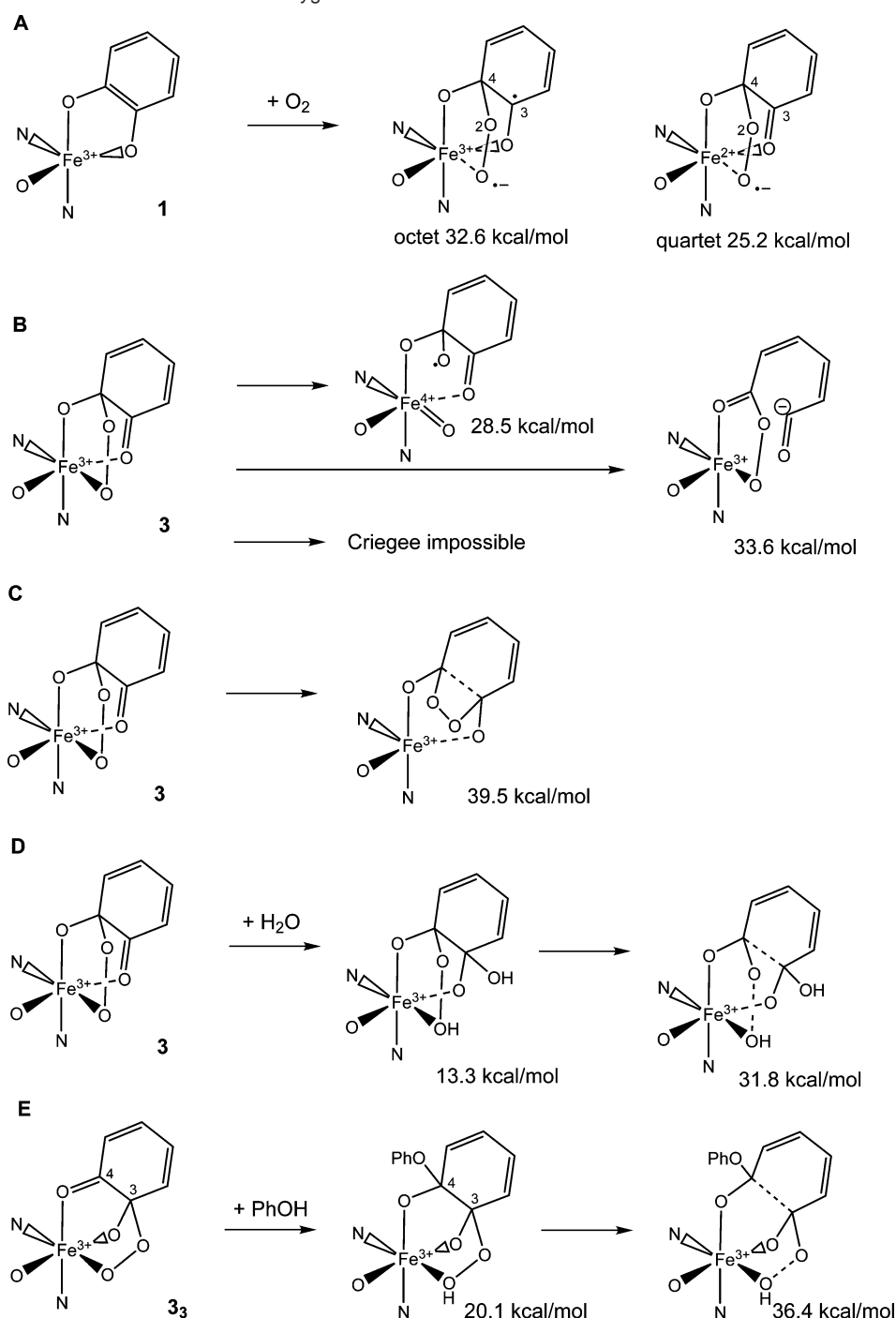
the important dihedral O1−O2−C4−C3 to ca. −180°, a process facilitated by the second-shell residues (Arg457, Gln477, and Tyr479), (4) binding of a neutral ligand XO−H (H₂O or Tyr447) at the open coordination site of **3′** and a proton transfer from XO−H to the peroxo group leading to species **5**, (5) a Criegee rearrangement (**TS**$_{Criegee}$) of **5** yielding the anhydride intermediate **6**, or, alternatively, a homolytic O−O bond cleavage coupled with electron transfer from Tyr408 to the hydroperoxo group (**TS**$_{ET}$), which through a metastable radical species **9** also leads to the anhydride **6**, and finally (6) the hydrolysis of **6** into the acyclic product complex **8** by the iron-bound hydroxide anion. This mechanistic proposal is in agreement with several experimental facts. First, the dioxygenase nature of the enzyme is

guaranteed by efficient incorporation of both atoms derived form dioxygen into the product. Second, the product specificity, i.e., the *intra* scission, is explained, but the presence of the homolytic path (**TS**$_{ET}$) opens the possibility for the formation of the minor *intra* cleavage product, as observed for some nonphysiological substrates.[26] Third, the role of the second-shell Arg457 is explained. Here, concerning the chemical reactions of the catalytic cycle, which are addressed in this paper, it is proposed that this charged residue together with its H-bonding partners (Gln477 and Tyr479) is engaged in the conformational change of the peroxo intermediate (**3** → **3′**). These second-shell residues provide 5.6 kcal/mol stabilization energy to the open structure (**3′**) and reduce by ca. 2 kcal/mol the barrier for the slowest

chemical step, i.e., the Criegee rearrangement. As for the dioxygen binding steps ($1 \rightarrow 3$), the presence of these second-shell groups has an impact on the electronic structure of species **1** (Figure 1), but the energy profile is hardly affected (Figure 2). Finally, species **6** is substantially stabilized due to an extra H bond present in **6** compared to **5** (see Figures 8A and 6A).

The inhibitory nature of 4-nitrocatechol is reproduced by the present calculations, as is the acceleration effect of the electron-donating ring substituents.[23,24] Finally, the mechanism advocated here incorporates two features of 3,4-PCD inferred from extensive structural research devoted to this enzyme.[2,18,19,22] First, the propensity of the active site to maintain the same total electric charge is incorporated into the mechanism. Second, the suggested mechanism makes use of the plasticity of the coordination environment of iron. Taken together, it is believed that the suggested mechanism has a sound basis, provides plausible explanation for a wide array of experimental observations and may stimulate further theoretical and experimental research aiming at understanding the mechanism of intradiol dioxygenases and their mimics. From a broader perspective, new insight into the mechanism of ring activation and the Criegee rearrangement have been provided by the computational results presented here, and these are believed to advance our understanding of the interesting catechol chemistry.

Supporting Information Available: Full author list for reference 29; Cartesian coordinates and calculated energies for all ground and transition state structures. This material is available free of charge via the Internet at http://pubs.acs.org.

JA0641251